Comprehensive Journal of Science
Volume (10), Issue (37), (NOV. 2025)
SICST2025, www.sicst.ly
ISSN: 3014-6266

مجلة العلوم الشاملة
عدد خاص بالمؤتمر الدولي الثالث للعلوم والتقنية
المجلد (10)، العدد (37)، (نوفمبر2025)
ردمد: 3014-6266

The Impact of Laser Irradiation Durations on Zinc Oxide Nanostructures' Crystallinity, Surface Morphology, and Electrical Properties in Palladium/Glass

Abdulwahab S.Z. Lahewil[1,2,3,*], Abdulmula Salem Z. Laheew[4], Daw Salem Alzarouq[1,2], Naser M. Ahmed[3,5]

[1]The Institute of Science and Technology of Al-Orban, Al-Orban Libya

[2]The Ministry of Technical & Vocational Education Tripoli, Libya

[3]School of Physics, Universiti Sains Malaysia (USM), 1800, Penang, Malaysia

[4]Libyan Authority for Scientific Research, Tripoli Libya

[5]Department of Medical instrumentation engineering, Dijlah university college, Baghdad, Iraq

*corresponding auther: lkmatys9@gmail.com

Received: 30-09-2025; Revised: 10-10-2025; Accepted: 31-10-2025; Published: 25-11-2025

Abstract: The LACBD technique is used to make ZnO nanostructures and thin layers of palladium (Pd) on glass. Crystallinity, surface morphology, and electrical characteristics were investigated at 20, 25, and 30 minutes of laser radiation. According to the XRD patterns, the generated ZnO-NSs are polycrystalline with a hexagonal/wurtzite structure and a preferential orientation along the c-axis, as observed on 002 planes. The thin surface was examined using a FE-SEM. The outcome indicates that the orientation and spatial growth of the nanostructure significantly depend on the presence of the Pd buffer layer. The findings showed that the polycrystalline ZnO-NSs' surface structures and topographical properties were significantly influenced by the duration of the laser irradiation. Keithley 2400 used to charactraze the photoelectric effects. Additionally, the efficiency of Pd/ZnO NSs/Pd in UV detection has been researched. Both in low light and UV radiation, the photodetector exhibits outstanding stability and reactivity.

Keywords: Pd, ZnO, LACBD, and irradiation of laser.

1. Introduction

Semiconductors have garnered a lot of interest in both technical and scientific applications as a significant class of material alternatives for optoelectronic devices and sensors [1]. ZnO is a semiconducting and piezoelectric substance with a high exciton binding energy of 60 meV and a comparatively wide band-gap of 3.37 eV at ambient temperature [2, 3]. These uses demonstrate ZnO's adaptability in several domains, such as energy

conversion, electronics, and piezoelectric transducers [5], as well as surface acoustic wave devices and environmental monitoring [6]. As research continues, the potential for innovative uses of ZnO is likely to expand even further. Examples of 1D ZnO nanostructures that have garnered a lot of interest lately in the realm of nanotechnology are nanotubes, nanobelts, and nanowires. ZnO nanowires (ZnO-NWs) have garnered significant interest for various applications in electronics, optoelectronics, and energy harvesting due to their distinct semiconducting, photonic, and piezoelectric characteristics [10-12]. Numerous optoelectronic, electrochemical, and electromechanical devices [13-15], including ultraviolet (UV) lasers, extremely efficient light-emitting diodes [18-19], and field emission devices [20], have shown benefits from ZnO-NWs. Excellent-performing nanosensors [21], solar cell panels are dye-sensitized by nanowire numerous methods, including wet chemical procedures, PVD, sputtering, pulsed laser deposition, LACBD, have been used to create one-dimensional (1D) ZnO nanostructures (NSs). A photoluminescence experiment was done on crystalline undoped ZnO nanostructures made using RF magnetron sputtering [26]. Traditional technic for generating 1-dimensional (1D) ZnO-NSs, for exameal whiskers, nanowires, vapor-solid (VS) nanorods, nanonails, and nanorings, mostly use growth and vapor-liquid-solid (VLS). During the initial growth stage, a metal catalyst creates the liquid phase [27, 28]. A somewhat high growth temperature is required for the VS and VLS processes. For instance, 750°C to 1300°C is the ideal temperature range for the growth of ZnO nanowires and nanorods [29, 30]. Furthermore, metal catalysts like Ni, Au, Sn, and Pd are contaminants that typically create unintentional trap levels in the semiconductor bandgap, which may lead to difficulties in using these materials for electronics and optoelectronics [31].

Using a LACBD technique, we characterized ZnO NSs in this study after post-annealing for three hours at 400 °C after 20, 25, and 30 minutes

respectively. Electrical, morphological, crystallographic, and structural characteristics were investigated in connection with laser irradiation duration. Specifically, we investigated the absorbance, rise time and decay time, photosensitivity, current gain, quantum efficiency, responsivity (R), Specific detectivity (D*), NEP, and EQE. We used an easy-to-use continuous-flow cavity design approach to create the ZnO NSs at low temperatures. Using XRD, FE-SEM, and I-V characteristics, high specific surface to volume ratio, micro area, and scalability flexibility were assessed. It has been demonstrated that the LACBD technique is a practical way to create nanostructures for sensing applications. It has been demonstrated that the Pd/ZnO NSs/Pd photodetector is a crucial component in the sensitive detection of Ultraviolet (UV) light.

2. Materials and Techniques Employed

The method of LACBD was used in this study to produce Zinc Oxide Nanostructures, which were then cultivated at 60°C. The properties of the deposited material were altered and controlled using the cavity flow method of chemical bath deposition (CBD) optimization. Zinc acetate dihydrate (99.99%), $Zn(CH_3COO)_2.(H_2O)_2$, and hexamethylenediamine (99.9%) were used to generate ZnO NSs (HMTM, $C_6H_{12}N_4$). The deposition solvent utilized was deionized water. Without any additional purification, all of the compounds were utilized just as they were purchased from Sigma Aldrich. A simple flow solution cavity, buffer layer activation, which is facilitated by continuous laser irradiation duration, was designed and built using LACBD technology. In this work, ZnO-NSs were grown at 60 °C after being created utilizing the LACBD technique. The cavity flow method of chemical bath deposition (CBD) optimization was used to modify and control the properties of the material that was deposited. ZnO NSs (HMTM, $C_6H_{12}N_4$) were produced, zinc acetate dihydrate (99.99%), $Zn(CH_3COO)2.(H_2O)2$, and hexamethylene-diamine (99.9%) was used. The

solvent for deposition was deionized water, without any additional purification, all of the compounds were utilized just as they were purchased from Sigma Aldrich. LACBD technic was used to develop and construct a straightforward flow solution cavity and buffer layer activation, which is made possible by a continuous laser irradiation period. Fig. 1 (a), and (b) present a schematic representation of the ZnO-NSs preparation method [32].

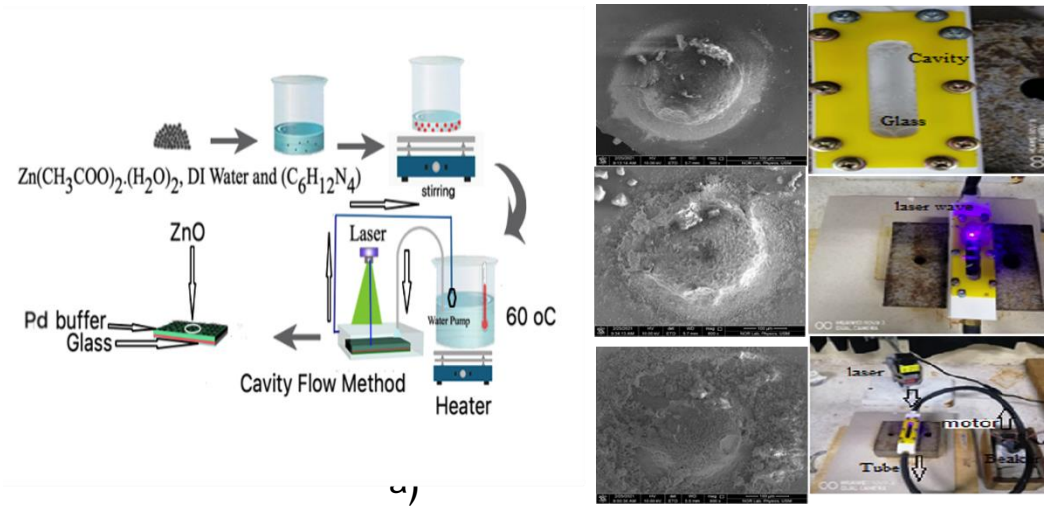

a)

b)

Figure 1 illustrates the scheme for creating ZnO NSs/Pd/Glass images using the LACBD technique at varying laser irradiation periods of 20, 25, and 30 minutes, respectively.

3. The Findings and Discussion

3.1. Structural Description

Laser Assisted Chamical Bath Deposition technique and post-annealing at 400°C for three hours was used. The ZnO-NSs formed on Pd buffer layers on glass substrates surface are displayed at Fig. 2. (a, b, and c) along with their XRD patterns at various laser irradiation periods at (20, 25, and 30 minutes). 2θ degree = 34.325° (002) ZnO, 40.225° (111) Pd, 47.575° (200) ZnO, 53.225° (102) ZnO, and 68.125° (112) ZnO, 34.275° (002) ZnO,

40.075° (111) Pd, 44.225° (200) Pd, 47.275° (102) ZnO, 64.725° (200) ZnO, 34.775° (002) ZnO, 40.075° (111) Pd, 47.857° (102) ZnO, 55.475° (110) ZnO, and 68.625° (112) ZnO, respectively, are represented by the XRD spectra's peaks. The hexagonal wurtzite also exhibits notable peaks at 2 = 34.375°, 34.275°, and 34.775°, which correspond to (Rf. Cod. 079-0208), as shown by the 3-specimens for the ZnO formed on the Pd buffer layer at (20, 25, and 30 minutes) of laser irradiation durations. However, the structures at diffraction angles of 2θ degree = 40.167°, 40.161°, and 40.111°, which correspond to the lattice planes (111) connected to the cubic crystalline of Pd (Ref. Cod. 03-065, 2867), showed notable intensity fluctuations, [33-35]. Due to the difference in atom radius between Zn (1.25) and Pd (1.28), the diffraction peaks of ZnO (002) and Pd (111) demonstrate that increasing the laser irradiation periods at (20, 25, and 30 minutes), causes lattice deformation. As well as the lattice interplanar spacing being approximately 0.1499, 0.1501, and 0.1482 nm, related to ZnO, while the lattice interplanar spacing for the Pd (111) plane is approximately 0.1204, 0.1202, and 0.1153 nm, respectively. The reaction that takes place when a solution of zinc acetate dihydrate is heated in a furnace has been the subject of numerous investigations [36,37].

$$c = \frac{\lambda}{\sin\theta} \quad (6)$$

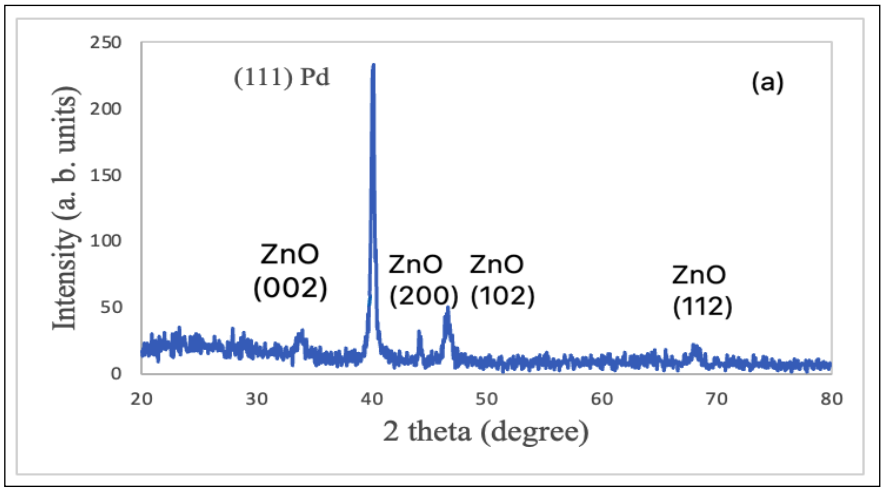

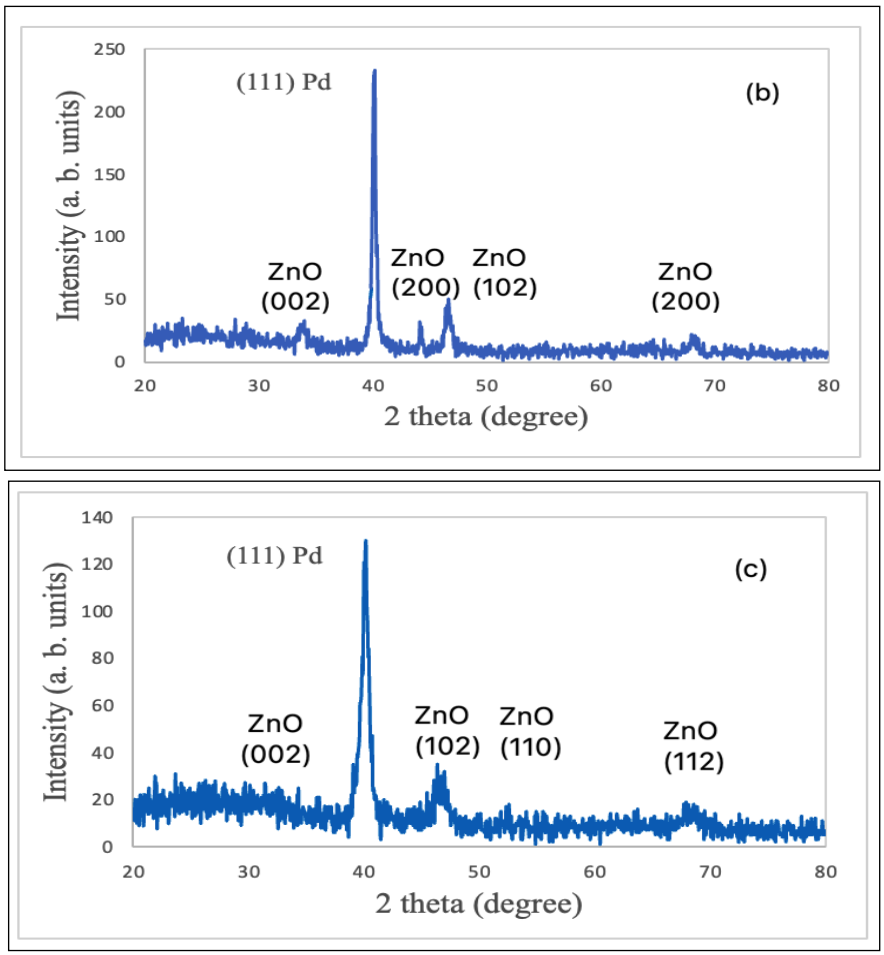

Figure 2 displayed the XRD results for these nanostructures' continuous laser irradiation for (a) 20, (b) 25, and (c) 30 minutes, followed by three hours of post-annealing at 400°C. ZnO nanostructures were formed on a glass substrate with a Pd buffer layer.

The average crystallite size (D) was calculated using Scherrer's formula (Eq. 1) and the structural

$$D = \frac{k\lambda}{\beta cos\theta} \quad (1)$$

where k is a constant of 0.94, θ is Bragg's angle, β is the X-ray's full width at half maximum (FWHM), and λ is its wavelength. The dislocation density (δ), as

determined by Eq. 2, is the quantity of dislocation line lengths per unit volume [33-35]:

$$\delta = \frac{1}{D^2} \quad (2)$$

Using Eq. (3), the strain (ε) of ZnO nanostructures was calculated [33-35]:

$$\varepsilon = \frac{\beta \cos\theta}{4} \quad (3)$$

Bragg's equation, Eq (4), is used to calculate the interplanar distance (*d*) [33,35].

$$d = \frac{h\lambda}{2\sin\theta} \quad (4)$$

where h is a constant that has the value 1. The low value of d observed in this work supports the good crystallinity of the ZnO nanostructure for all sets. Equations (5) and (6) were used to determine the lattice constants (a) and (c) [33-35].

$$a = \frac{\lambda}{\sqrt{3}\sin\theta} \quad (5)$$

$$c = \frac{\lambda}{\sin\theta} \quad (6)$$

Table 1 displays the ZnO/Pd/glass nanostructures XRD data at various laser irradiation periods of 20, 25, and 30 minutes after three hours of annealing at 400°C.

Laser irradiation time (min)	*Peak 2θ (degree)*	*Grains Size (D) (nm)*	*Dislocation density (δ) 10^{14}*	*Strain (ε) (10^{-3})*	*Inter planer distance (d) (Å)*	*Lattice Constant a=b, c (Å)*

			lines/m²			
	34.325°	8.4346	0.014056	0.0429	1.499721	*a* = 1.73
	44.175°	2.690	0.13819	0.13453	1.20406	*c* = 2.99
20	46.675°	2.0507	0.2378	0.1764	1.15058	*a*= 1.39
	68.325°	15.1653	0.00434	0.0238	0.8762	*c* = 2.40
						a = 1.329 *c* = 2.302
						a = 1.012 *c* = 1.753
	34.275°	16.861	0.003517	0.0214	1.501692	*a* = 1.734 *c* = 3.004
	44.225°	3.4259	0.0852	0.10563	1.2028	
25	46.625°	7.787	0.01649	0.04647	1.15158	
	68.325°	15.1653	0.00434	0.0238	0.8762	*a* = 1.389 *c* = 2.406
						a = 1.012 *c* = 2.303
						a = 1.012 *c* = 1.753
	34.775°	8.4706	0.013936	0.0427	1.48224	*a* = 1.712 *c*
	46.525°	12.9603	0.00595	0.02792	1.1536	

30	52.575°	10.676	0.00877	0.033896	1.04744	= 2.965
	67.775°	14.93	0.004487	0.01891	0.83179	$a = 1.332\ c = 2.308$ $a = 1.210\ c = 2.090$ $a = 0.961\ c = 1.663$

3.2 Study of the Morphology

Field emission scanning electron microscopy used to analyze the surface morphologies of the thin films that were deposited. Figure 3 displays top views of ZnO nanostructures after they have been post-annealed at 404 °C for 3h after being exposed to laser light for (20, 25, and 30 minutes). Nanostructures ZnO look densely packed, evenly aligned nanobelts-like, nanoflowers-like, and nanopetal-like. Under laser spot areas, the grains are connected to one another and each sample has a excellence grain boundary. The NSs' morphology was clearly altered by laser irradiation durations at 20, 25, and 30 minutes on the specific area under the laser irradiation spot, even if the top-view photos indicate the new growth, of a dome structure. As well defined grain boundaries in the densely packed NSs in the laser irradiated ZnO NSs. Some of the ZnO NSs did not aggregate with other grains after the time of laser irradiation increased to (20 min, 25 min, and 30 min) respectively.

1. 2.

3

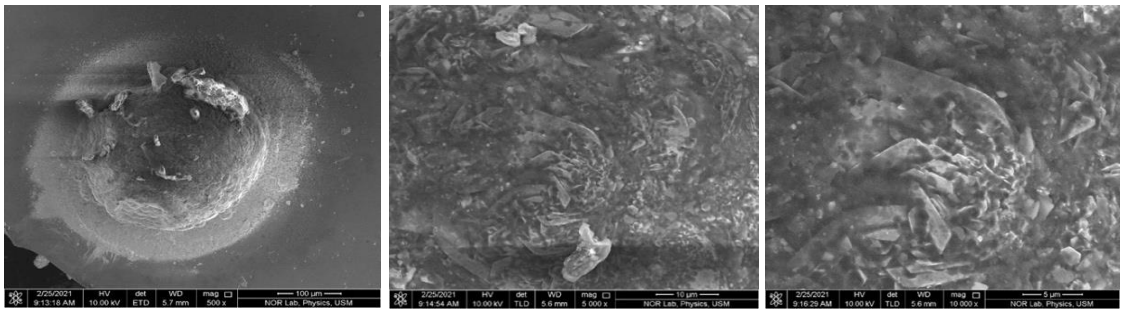

(a)

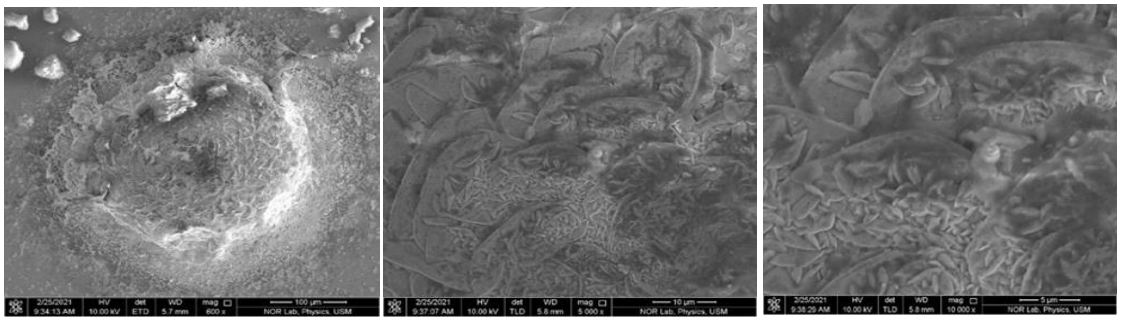

(b)

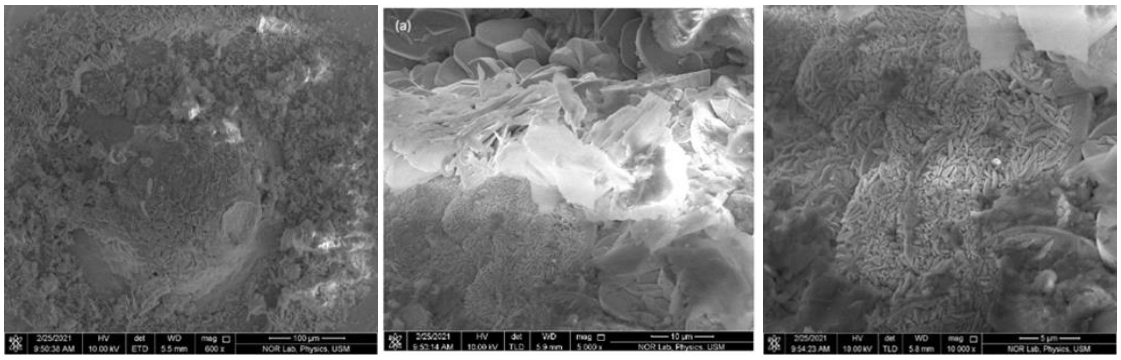

(c)

Figure 3: FE-SEM top-view pictures at different magnifications for the ZnO/Pd buffer layer formed on glass substrates during laser irradiation periods of (a), (b), and (c) of 20, 25, and 30 minutes, respectively, with post-annealing at 400°C for three hours are shown in (a1), (b1), and (c1).

4. Electrical Characteristics

4.1. UV Photoconductive Characterization

Keithley 24000 current source unit using and coupled to a computer for data processing, the typical I-V curve of a UV photodetector (Pd/ZnO/Pd/glass) in a ZnO NSs-based MSM design was examined. By changing the bias voltage from -5V to 5V, Ohmic behavior was seen in the I-V characteristic curve of the (Pd/ZnO-NSs/Pd) glass structure in the forward bias, as shown in Fig. 4. As a proof of concept, ZnO-NSs' capacity to detect UV light was examined by simply observing how their electrical responses changed when exposed to UV light. At a slot width of 0.5 mm, it was discovered that clusters of ZnO-NSs actually served as a bridge connecting the two Pd pads. To establish a metal contact, ZnO-NSs were cultivated using the LACBD approach in the area between the Pd pads. The ZnO-NSs UV photodetector had an active diameter of about one millimeter. The photoelectrical characteristics of UV photodetectors were examined using a two-point probe. The light source for the ultraviolet light illumination was a light-emitting diode (LED) with a central UV illumination wavelength of 380 nm and an intensity of 0.7186 mW/cm² at room temperature in an ambient atmosphere.

Dark current (I_d) is so weak compared, to photocurrent (I_{ph}) that it is subtracted from the latter to determine the net photocurrent ($I_{ph} = I_{light} - I_{dark}$) [47]. The distinction between photocurrent and dark current can be easily made. UV light causes the forward bias voltage to increase, which causes the

current to increase as well. However, it is clear that the forward current is stronger in the light than the dark current. The dark current for samples collected after 20, 25, and 30 minutes increased when a −5V reverse bias voltage was applied, to be 3.20 uA, 4.29 mA, and 1.32 mA, and the photocurrent was 17.16 uA, 5.92 mA, and 2.10 mA. Pd pad contact electrodes are necessary for the rapid collection and transport of photoelectrons from ZnO NSs. Oxygen chemisorption controls the ZnO-NSs thin film layer's photosensitivity in UV sensing experiments. On the surface of the ZnO-NSs thin film layer, oxygen molecules from the surrounding air adsorb as negatively charged ions after absorbing free electrons from the n-type ZnO in the absence of light. Consequently, a patch of low conductivity depletion develops on the surface of the thin film. Electron-hole pairs are produced when UV energy is absorbed by ultraviolet light. These electron-hole pairs travel across the surface of the film due to surface electron-hole recombination, which releases the adsorbed oxygen ions. The fact that most of the carriers' electrons are still inside the device also helps with the photocurrent [47].

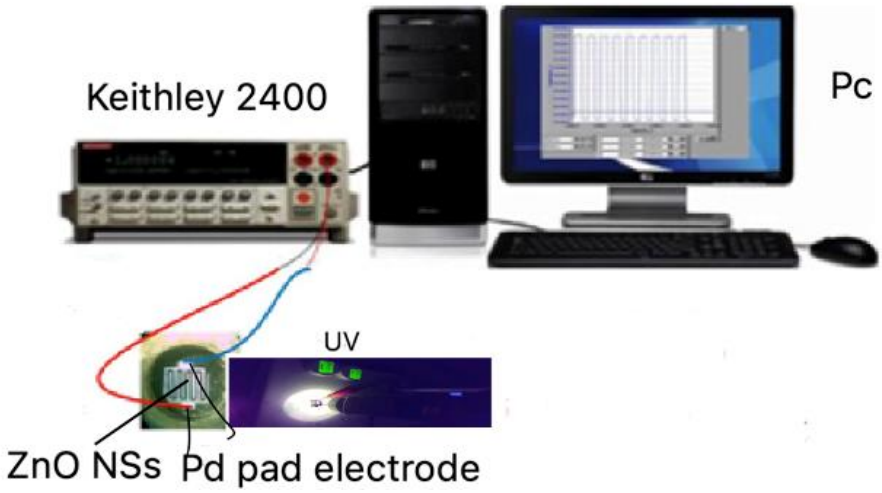

Figure 4. depicted the Keithley 2400 electrical system for assessing the electrical characteristics of UV photodetectors.

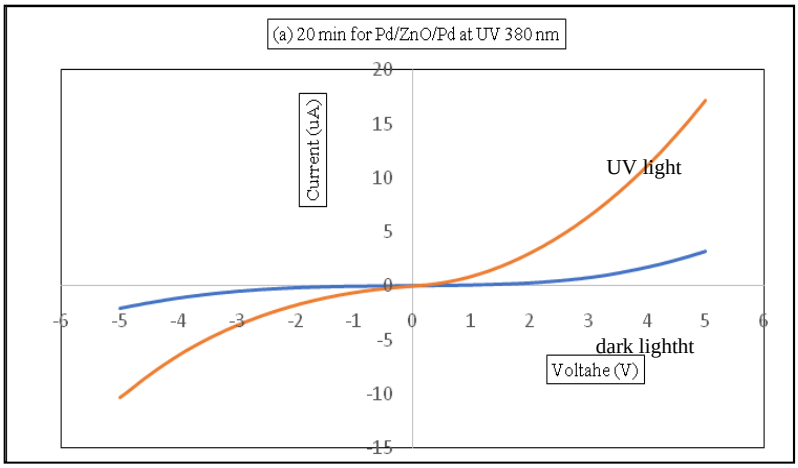

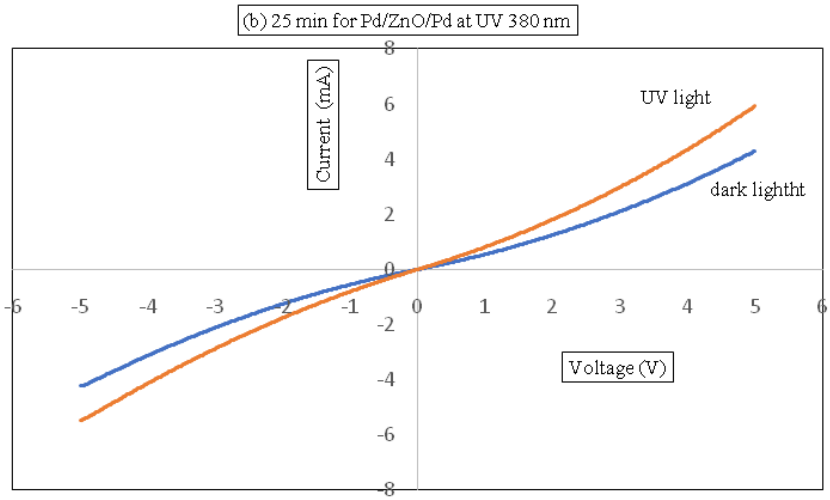

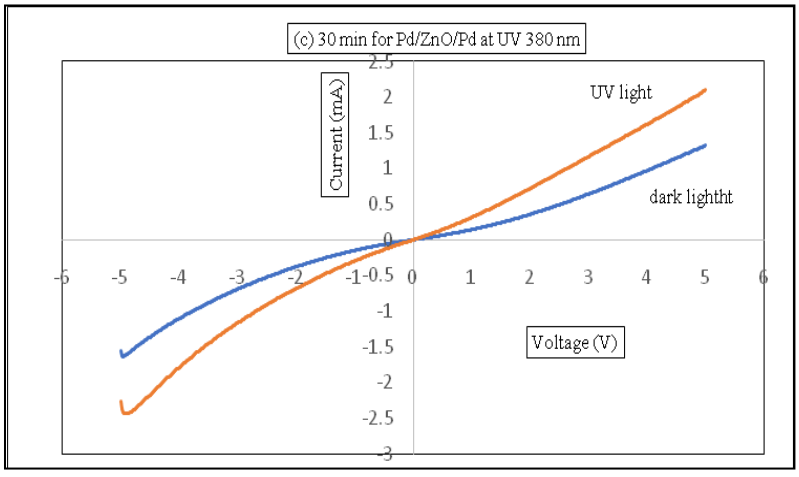

Figure 5 shows the Pd/ZnO NSs/Pd/glass photodetector device's I-V forward bias graphs after 20 (a), 25 (b), and 30 (c) minutes of laser irradiation, respectively.

The current as a function of time at various laser irradiation intervals of 20, 25, and 30 minutes, respectively, characterizes the device's reaction behavior. On all films, the transient curves are captured between 5.53s and 7.35s, 6.93s and 7.50s, and 6.64s and 7.51s after the device has been periodically exposed to UV radiation. Figure 5 displayed the device's time-resolved photo response of curve current in both the "on" and "off" states (a-c). With a reasonable time gap, the results show excellent consistency and repeatability. Each on/off cycle's photocurrent magnitudes had rectangular curves and were consistent and predictable. The MSM UV photodetector has repeatable characteristics ZnO-based NSs have a maximum photo response of 5.92 mA at a bias voltage of -5V. The photocurrent stays in the device long after the light has been turned off. Understanding the rise and fall timings of the photocurrent is necessary to ascertain the kinetics of the detector's response to a rapidly fluctuating optical input. The time needed to increase the photocurrent from 10% to 90% of its maximum value (r = 90% - 10%) is known as the rise time (r), and the time needed to decrease it from 90% to 10% of its maximum value (d = 10% - 90%) is known as the decay time (d = 10% - 90%) [48]. Under UV light, photocurrent initially rises quickly before steadily climbing to its maximum. When the light is switched off, the current rapidly decreases before gradually increasing to a value that is only slightly greater than the initial value. The continuing photoconductivity effect causes the current levels to be somewhat higher after each cycle. Because of the photoconductivity effect, the photocurrent in the detector keeps flowing even after the UV source is turned off. The photoconductivity effect prevents the photocurrent from returning to its starting value when there is no light present.

As indicated earlier, surface electron-hole recombination is a component of the photodetection approach. At this point, a few holes start to appear on the film's surface, which stops them from taking part in the recombination process. Without holes, electrons in the trap centers or conduction band cannot recombine. As a result, many electrons remain available in the conduction band (CB) and at the trap centers even after the UV source has been turned off. In the absence of light, free electrons (e^-) from the conduction band (CB) are drawn to oxygen atoms that adhere to ZnO NS surfaces. A oxygen ions is created the depletion zone with grain boundaries, which are known to be crucial for the light response, were used to quantify the current over time using a bias voltage of -5V [48]. In the dark, oxygen molecules adsorbed on the surface of ZnO NSs absorb free electrons from the n-type ZnO semiconductor, producing O_2 [O_2 (g) + e $\rightarrow$ O_2 (ad)]. This process results in upward band bending at the surface, a decrease in carrier density in the NRs, and the development of low-conductivity depletion layers that limit the mobility of the remaining carriers. When exposed to UV light at photon energies above the semiconductor bandgap, the carrier density in the nanowire structures increased. The performance of photodetectors can be assessed using the relationship below [47-48]. The MSM's shape, which produces a limited, exposed surface area, makes it architecturally appropriate for various applications. This demonstrates the enormous potential of such a technique for high-volume production, particularly for applications like sensors where high surface-to-volume ratios are essential to performance. According to the literature, surface oxygen absorption and desorption, which alters ZnO conductivity, is the main basis for the photodetection mechanism in ZnO structures. It has been demonstrated that the size of the ZnO exposed zone and native ZnO defects, such as oxygen and zinc vacancies, have a major impact on the outcomes [49]. A local electric field separates the electron-hole

pairs, and (h^+) from adsorbed oxygen ions (O^+) moves to the ZnO NSs' surface to recombine with (e^-). As a consequence, oxygen atoms on the ZnO NSs surface are released. Photoconduction is made easier by the CB's abundance of photogenerated electrons. The combined effects of photogenerated electron conduction and UV photodesorption of O_2 molecules lead to a considerable increase in the total conductivity of the ZnO NSs layer. When the device is in the on/off state, the electron density in the conduction band rises with each cycle. The electron density in the conduction band rises in tandem with the photocurrent with each cycle.

$$R = \frac{Iph}{P} \quad (12)$$

P is the intensity of illumination in the active region of the device, I_{ph} is photocurrent, and R is responsiveness. As the length of laser irradiation increases, Table 2 shows how the UV photodetectors with ZnO-NSs bases react. Performance of the response depends on the height of the stability of the Ohmic barriers [22]. Furthermore, the existence of a wide depletion breadth may influence responsiveness enhancement. Figure 5.b shows the device's highest responsivity of 2.324 A/W at a film formed after 25 minute of laser irradiation times. This level of responsiveness is improved compared to that reported by Boruah, Buddha Deka, et al. 2019 [49] and comparable to ZnO photodetectors reported by other researchers [47], Yuqiang Li, 2016 and 2020 [39, 53].

A single incoming photons contribution to the electron-hole bias, or quantum efficiency, is denoted as:

$$\eta = \frac{Iph/e}{P/hv} = R\,\frac{hc}{\lambda e} \quad (13)$$

Where R stands for responsiveness, h for plank constant, for wavelength, c for light speed, and e for elementary charge. However, Eq. (14) [47] assesses the UV photodetector photoresponse performance using the sensitivity factor (S):

$$S\ \% = \frac{Iph - Id}{Id} x\ 100\% \quad (14)$$

The determined sensitivity values are shown in the Table 2. It's significant to note that this research's sensitivity is higher than that of earlier studies that used TiO_2 nanostructures as photodetectors [47]. Our research shows that ZnO-NSs perform UV detection substantially better than other ZnO-NSs or thin films. ZnO nanostructures can collect free electrons and adsorb oxygen molecules due to their high surface area to volume ratio. As a result, the photo responsiveness will be very high. Equation (15) is used to calculate the current gain, which is calculated by dividing the number of photons absorbed to form photoelectrons per unit time by the number of electrons collected per unit time.

$$G = \frac{Iph}{Id} \quad (15)$$

Furthermore, detectivity is a crucial factor to consider when assessing a photoreactor's capacity to pick up a faint signal. The specific detectivity (D*) is calculated using equation (16) as shown below [47]:

$$D^* = R \sqrt{\frac{Ao}{2eId}} \quad (16)$$

Where, (R) denotes responsiveness, (A_o) the area of the photodetector that is expos ed to UV light, (e) the elementary charge unit, and (I_d) the dark current getting the best possible signal-to-noise ratio is the key issue with UV detectors. Note that Figures 6(a), (b), and (c) only apply to low bias voltages; the noise became smoother as the bias voltage rose. These figures depict a

variety of significant noise kinds, such as short noise, generation recombination noise, thermal noise, and others. the generation recombination noise spectrum is flat until the frequency values are almost equivalent to the inverse value of the free carrier lifetime. When samples were subjected to 380 nm UV light, the ZnO NSs photodetector's low noise equivalent power (NEP) was determined at the bias voltage of (−5V). The noise was largely caused by ionized defects and acoustic phonons, which cause mobility variation through lattice and impurity dispersion [32]. This could have an impact on a number of contaminants in our sample, including interstitial zinc and oxygen vacancies.For photodetectors, the NEP is a crucial quantity. It is the lowest optical power at which a photodetector can distinguish itself from noise. As a result, the following Eq. (17) may be used to calculate NEP:

$$NEP = \frac{\sqrt{Ao}}{D*} \quad (17)$$

$$EQE = \frac{hcR}{q\lambda} \quad (18)$$

Equation (18), where c is the speed of light, q is the electron charge, h is Planck's constant, and λ is the incoming wavelength, is used to calculate the external quantum efficiency (EQE). The detector's illumination of 0.7186 mW/cm² and a bias voltage of −5 V provide excellent performance.

Figure 6 shows the films made of Pd/ZnO NSs/Pd photodetectors at varying laser irradiation times of 20 (a), 25 (b), and 30 minutes (c).

The performance of our devices suggests that by employing LACBD to synthesize ZnO NSs, photodetectors with increased performance can be developed using an elaboration process. The key parameters for the (Pd−ZnO NSs−Pd)/Glass UV photodetector for bias voltages (−5V) of three samples made at various laser irradiation intervals of 20, 25, and 30 minutes,

respectively, are determined using the results in Figs. 5 and 6. Our ZnO NSs device demonstrated good UV sensitivity, a fast reaction time, and high response. these characteristics are linked to ZnO NSs's structure, high length-to-diameter ratio, and crystal quality, all of which are essential for the electrical characteristics of ZnO NSs devices [53]. The results demonstrate the potential for an ambient light optical switch based on a ZnO NSs-based MSM UV photodetector. When the applied electric field comes into touch with light, photogenerated charges are produced. The structure, high length-to-diameter ratio, and crystal quality of ZnO NSs are associated with these properties, and they are all necessary for the electrical properties of ZnO NSs devices. In general, a UV photodetector's sensitivity is mostly determined by its responsiveness (R) and sensitivity (S). Responsiveness is the ratio of the photocurrent on the device to the incident optical power. At a bias voltage of -5, the response and decay times of the UV detector were recorded. Table 2 clearly demonstrates how soon the increase and drop times were finished. The observed photocurrent in both the on and off modes increased quickly in response to UV exposure, whereas the current in the dark significantly dropped. Our ZnO-NSs device has high responsivity, quick response, and UV sensitivity that are similar to those of earlier ZnO-based UV detectors with glass substrates reported in the literature. Over time, the MSM device's (Pd/ZnONSs/Pd)/glass performance has stayed essentially unchanged. After several cycles, the maximum current value remained constant, indicating the stability and dependability of the photodetector. It's important to note that prolonged outdoor light exposure has no effect on the device's functionality. The Nanostructures' substantial surface area is an essential advantage because UV detection is a surface-based operation. To completely understand how ZnO nanostructures behave when exposed to UV light and to identify the factors that influence sensitive performance, more research is required into the

concentration of initial nanostructures' dispersion, the shape of interdigitated electrode detecting areas, Ohmic connections, and other features. The performance of our devices indicates that a straightforward and inexpensive elaboration method can be used to produce photodetectors with improved performance by using LACBD to create ZnO-NSs. Using the information in Figs. 5 and 6, determine the critical values for the (Pd/ZnO NSs/Pd)/Glass UV photodetector at a low voltage of (-5v) at various of laser irradiation periods.

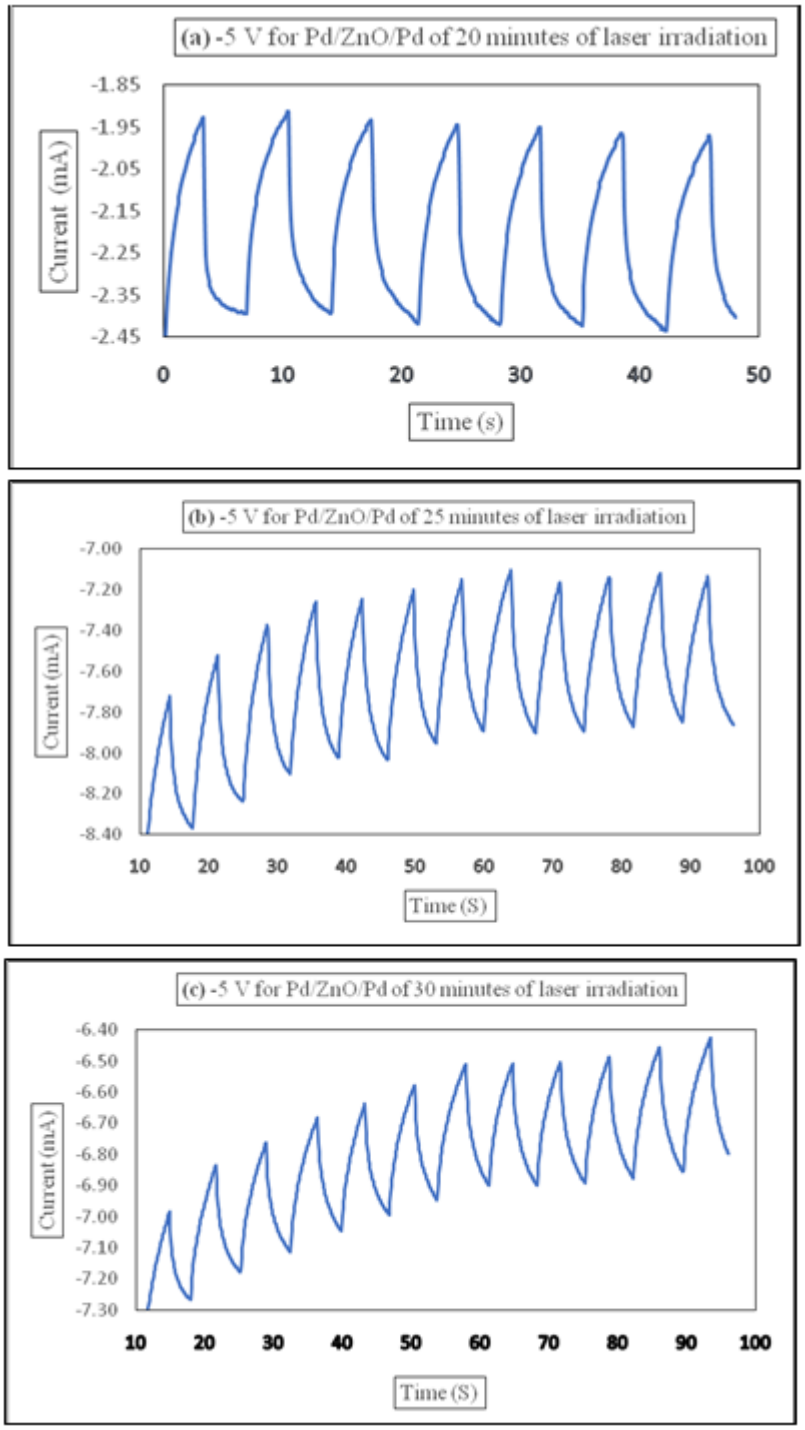
(a) -5 V for Pd/ZnO/Pd of 20 minutes of laser irradiation
Current (mA)
-1.85
-1.95
-2.05
-2.15
-2.25
-2.35
-2.45
0
10
20
30
40
50
Time (s)
(b) -5 V for Pd/ZnO/Pd of 25 minutes of laser irradiation
Current (mA)
-7.00
-7.20
-7.40
-7.60
-7.80
-8.00
-8.20
-8.40
10
20
30
40
50
60
70
80
90
100
Time (S)
(c) -5 V for Pd/ZnO/Pd of 30 minutes of laser irradiation
Current (mA)
-6.40
-6.50
-6.60
-6.70
-6.80
-6.90
-7.00
-7.10
-7.20
-7.30
10
20
30
40
50
60
70
80
90
100
Time (S)

Table 2: The electrical characteristics parameters of UV photodetectors based on Pd/ZnO NSs/Pd device, Bias voltage is −5V, and UV−illumination lambda (λ) is 380 nm.

Laser irradiation times film	τ_r (sec)	τ_d (sec)	R (A/W)	S %	G	η (%)	10^9D* (jones)	NEP (watt)	EQE %	Ref.
20 minutes	3.56	3.46	92.25806	436.25	5.3625	159288	2.996607	0.3337	7.75x10^−48	Current study
25 minutes	3.56	3.75	8.23824	37.995339	1.3799533	142237	0.2675839	3.7371	2.689x10^−11	Current study
30 minutes	3.45	3.85	2.922349	59.0909	1.590909	505076	0.09491998	10.535	9.541x10^−12	Current study
NiO/ZnO −5 v 310 nm		–	21.8	100	–	–	1.60 x10^12	–		*Boruah, Buddha Deka.2019*
Graphene /ZnO NW/Graphene −5v / 365 nm	3.0	0.47	23.0	–	–	–	–	–		*Boruah, Buddha Deka. 2019*
Si3N4/Si	–	–	0.325	–	–	–	–	–	218	*Yuqiang Li, 2020*

4.2. The mechanism of photoconduction in UV photodetectors made from ZnO NSs

The surface of nanostructures strongly influences the electrical and optoelectronic properties of nanodevices. Surface states affect luminescence, gas sensing, optical absorption, and other properties due to the high surface−to−volume ratio. As a result, compared to bulk materials, nanoscale electrical devices ought to be able to achieve higher sensitivity and quicker reaction times. For the majority of these applications, receiving and sending electrical impulses requires metal contact or outside force. Therefore, the scale of the

electrical connections in nanowire, nanorod, nanobelt, or nanotube-based systems should be acceptable. Therefore, it is crucial to comprehend transport processes at the nanoscale in order to enhance device characteristics generally. Because of the photoconductivity effect, the photocurrent in the detector keeps flowing even after the UV source is turned off. As previously reported, surface electron-hole recombination takes place during the photodetection process. Holes start to show up at the film surface at this stage and are unable to participate in the recombination process. Due to the absence of holes, electrons trapped in the conduction band (CB) or at the trap centers cannot be involved in future recombination. As a result, many electrons remain accessible in the CB and at the trap centers even when the UV source is switched off. In the absence of light, oxygen molecules attach to the ZnO-NSs' surface after stealing free electrons (e) from the CB [53].

O_2 (gas) + e- (surface) ---------- O^-_2 (adsorption)

When exposed to UV light with photon energy (hv) greater than the ZnO bandgap (hv > Eg), the ZnO-NSs surface layer creates electron-hole pairs. A modest electrical field separated the electron-hole pairs (h+) from adsorbed oxygen ions, which then migrated to the surface of ZnO-NSs to recombine with (e-). Thus, oxygen atoms are liberated from the surface of ZnO-NSs. The photoconduction of CB is facilitated by the presence of photogenerated electrons [50]. h^+ (hv) + O^-_2 (adsorption) --------- O_2 (gas)

The conduction of photogenerated electrons and the total conductivity of ZnO NSs are significantly improved by the synergistic action of UV photodesorption of O_2 molecules by activating holes. When the CB is in the on-off state, it is clear that its electron density increases with each cycle. The increase in photocurrent that occurs after each cycle is linked to the CB's greater electron density [51]. A ZnO-NSs-based UV photodetector's

photoconduction mechanism is shown in Figure 7, while UV radiation is shown in Figure 7.a. The bottom schematic shows the adsorption of oxygen atoms on the surface of ZnO-NSs in dark Fig. 7b, with upward energy band banding, valence and conduction bands, and the presence of surface trap states. Additionally, it is evident that oxygen molecules are drawn to ZnO-NS surfaces. Photogenerated holes reduce the low conductivity depletion width when exposed to UV light by migrating to the nanostructure surface along the potential slope caused by energy band bending for the desorption of adsorbed oxygen molecules. Figure 7c illustrates the migration of photogenerated holes for oxygen desorption and the decrease in upward energy band bending at the bottom following UV treatment. The oxygen molecules are reabsorbed when the UV irradiation light is switched off, and vice versa [52,53].

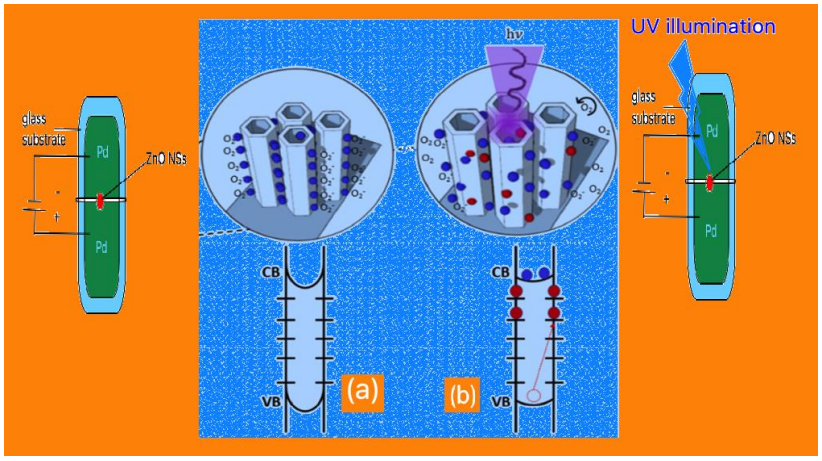

Figure 7: A UV photodetector based on ZnO-NSs is shown schematically in (a) where oxygen molecules adsorb on the material's surface in the dark and (b) where electron-hole pairs are photogenerated in response to UV illumination.

5. Conclusion

Using the LACBD approach, successful ZnO morphology structures were constructed and deposited on Pd buffer layers on polycrystalline, adherent, and homogeneous glass substrates. The relationship between the

length of laser irradiation and the micro-nanostructures, nanoparticle morphology, and crystallinity of ZnO-NSs/Pd/glass has been studied. The improved readings at faster nanoflower growth rates could be due to the ZnO-NSs' improved surface shape and crystallinity. According to the study's findings, the LACBD method is a promising technology that could be used in sensing applications because of its low synthesis temperature, short manufacturing time, and sufficient purity and homogeneity. It can be irradiated for 20, 25, and 30 minutes. Its use in photodetector devices has also been demonstrated when Pd/ZnO NSs/Pd SMS is made for UV sensing. Industrial applications are expected to improve as a result of fewer steps in the process and, the faster growth rate. When the exposed to 380 nm light (0.7186 mw/cm²), the developed, UV detector. showed excellent sensitivity, a strong photocurrent, and outstanding long-term stability. It could be produced at a reasonable cost for commercial photoelectronic uses.

Acknowledgment

The School of Physics at Universiti Sains Malaysia (USM), the Institute of Science and Technology of Al-Orban, Al-Orban, Libya, and the Ministry of Technical & Vocational Education, Tripoli, Libya, provided the research facilities and support, for which the authors are grateful.

References

1. Talapin, Dmitri V., Nikolai Gaponik, Holger Borchert, Andrey L. Rogach, Markus Haase, and Horst Weller. "Etching of colloidal InP nanocrystals with fluorides: photochemical nature of the process resulting in high photoluminescence efficiency." The Journal of Physical Chemistry B, 106, no. 49 (2002): 12659-12663.
2. Özgür, Ümit, Ya I. Alivov, Chunli Liu, A. Teke, MAnReshchikov, S. Doğan, V. C. S. J. Avrutin, S-J. Cho, and and H. Morkoç. "A comprehensive

review of ZnO materials and devices." Journal of applied physics, 98, no. 4 (2005): 11.

3. Choudhary, Shipra, Kavita Sahu, Aditi Bisht, BiswarupSatpati, and Satyabrata Mohapatra. "Rapid synthesis of ZnO nanowires and nanoplates with highly enhanced photocatalytic performance." Applied Surface Science, 541 (2021): 148484.
4. Minne, S. C., S. R. Manalis, and C. F. Quate. "Parallel atomic force microscopy using cantilevers with integrated piezoresistive sensors and integrated piezoelectric actuators." Applied Physics Letters, 67, no. 26 (1995): 3918-3920.
5. Chen, T. L., D. S. Ghosh, D. Krautz, S. Cheylan, and V. Pruneri. "Highly stable Al-doped ZnO transparent conductors using an oxidized ultrathin metal capping layer at its percolation thickness." Applied Physics Letters, 99, no. 9 (2011): 181.
6. X. Y. Du, Y. Q. Fu, S. C. Tan, J. K. Luo, A. J. Flewitt, S. Maeng, S.H. Kim, Y. J. Choi, D. S. Lee, N. M. Park, J. Park, W.I. Milne,"ZnO film for application in surface acoustic wave device." In Journal of Physics: Conference Series, vol. 76, no. 1, p. 012035. IOP Publishing, 2007.
7. Yuan, Hongtao, and Yao Zhang. "Preparation of well-aligned ZnO whiskers on glass substrate by atmospheric MOCVD." Journal of crystal growth, 263, no. 1-4 (2004): 119-124.
8. Zhang, Xian-Hua, Su-Yuan Xie, Zhi-Yuan Jiang, Xuan Zhang, Zhong-Qun Tian, Zhao-XiongXie, Rong-Bin Huang, and Lan-Sun Zheng. "Rational design and fabrication of ZnO nanotubes from nanowire templates in a microwave plasma system." The Journal of Physical Chemistry B, 107, no. 37 (2003): 10114-10118.
9. Ghafouri, Vahid, Akbar Ebrahimzad, and Mohsen Shariati. "The effect of annealing time and temperature on morphology and optical properties of

ZnO nanostructures grown by a self-assembly method." Scientia Iranica, 20, no. 3 (2013): 1039-1048.

10. Xu, Sheng, Chen Xu, Ying Liu, Youfan Hu, Rusen Yang, Qing Yang, Jae-Hyun Ryou et al. "Ordered nanowire array blue/near-UV light emitting diodes." Advanced materials, 22, no. 42 (2010): 4749-4753.
11. Wang, Zhong Lin, Rusen Yang, Jun Zhou, Yong Qin, Chen Xu, Youfan Hu, and Sheng Xu. "Lateral nanowire/nanobelt based nanogenerators, piezotronics and piezophototronics." Materials Science and Engineering: R: Reports, 70, no. 3-6 (2010): 320-329.
12. Zimmler, Mariano A., Federico Capasso, Sven Müller, and Carsten Ronning. "Optically pumped nanowire lasers: invited review." Semiconductor Science and Technology, 25, no. 2 (2010): 024001.
13. Wang, Zhong Lin. "Oxide nanobelts and nanowires-growth, properties and applications." Journal of nanoscience and nanotechnology, 8, no. 1 (2008): 27-55.
14. Wang, Zhong Lin. "Splendid one-dimensional nanostructures of zinc oxide: a new nanomaterial family for nanotechnology." ACS nano 2, no. 10 (2008): 1987-1992.
15. Zhang, Chunfeng, Fan Zhang, Tian Xia, Nitin Kumar, Jong-in Hahm, Jin Liu, Zhong Lin Wang, and Jian Xu. "Low-threshold two-photon pumped ZnO nanowire lasers." Optics express, 17, no. 10 (2009): 7893-7900.
16. Ma, Xiangyang, Jingwei Pan, Peiliang Chen, Dongsheng Li, Hui Zhang, Yang Yang, and Deren Yang. "Room temperature electrically pumped ultraviolet random lasing from ZnO nanorod arrays on Si." Optics Express, 17, no. 16 (2009): 14426-14433.
17. Govender, Kuveshni, David S. Boyle, Paul O'Brien, David Binks, Dave West, and Dan Coleman. "Room-temperature lasing observed from ZnO

nanocolumns grown by aqueous solution deposition." Advanced Materials, 14, no. 17 (2002): 1221-1224.

18. Govender, Kuveshni, David S. Boyle, Paul O'Brien, David Binks, Dave West, and Dan Coleman. "Room-temperature lasing observed from ZnO nanocolumns grown by aqueous solution deposition." Advanced Materials, 14, no. 17 (2002): 1221-1224.
19. Zimmler, Mariano A., Daniel Stichtenoth, Carsten Ronning, Wei Yi, Venkatesh Narayanamurti, Tobias Voss, and Federico Capasso. "Scalable fabrication of nanowire photonic and electronic circuits using spin-on glass." Nano letters, 8, no. 6 (2008): 1695-1699.
20. Wang, Wen-Zhong, Bao-Qing Zeng, Jian Yang, Bed Poudel, J. Y. Huang, Michael J. Naughton, and Z. F. Ren. "Aligned ultralong ZnO nanobelts and their enhanced field emission." Advanced Materials, 18, no. 24 (2006): 3275-3278.
21. Zhou, Jun, Yudong Gu, Youfan Hu, Wenjie Mai, Ping-Hung Yeh, Gang Bao, Ashok K. Sood, Dennis L. Polla, and Zhong Lin Wang. "Gigantic enhancement in response and reset time of ZnO UV nanosensor by utilizing Schottky contact and surface functionalization." Applied physics letters, 94, no. 19 (2009): 191103.
22. Yao, B. D., Y. F. Chan, and N. Wang. "Formation of ZnO nanostructures by a simple way of thermal evaporation." Applied physics letters, 81, no. 4 (2002): 757-759.
23. Heo, Y. W., V. Varadarajan, M. Kaufman, K. Kim, D. P. Norton, F. Ren, and P. H. Fleming. "Site-specific growth of ZnO nanorods using catalysis-driven molecular-beam epitaxy." Applied physics letters, 81, no. 16 (2002): 3046-3048.
24. Hong, Jung-Il, Joonho Bae, Zhong Lin Wang, and Robert L. Snyder. "Room-temperature, texture-controlled growth of ZnO thin films and their

application for growing aligned ZnO nanowire arrays." Nanotechnology, 20, no. 8 (2009): 085609.

25. Chiou, Wen-Ting, Wan-Yu Wu, and Jyh-Ming Ting. "Growth of single crystal ZnO nanowires using sputter deposition." Diamond and Related Materials, 12, no. 10-11 (2003): 1841-1844.
26. Sui, X. M., C. L. Shao, and Y. C. Liu. "White-light emission of polyvinyl alcohol/ ZnO hybrid nanofibers prepared by electrospinning." Applied Physics Letters, 87, no. 11 (2005): 113115.
27. Wu, J-J., and S-C. Liu. "Low-temperature growth of well-aligned ZnO nanorods by chemical vapor deposition." Advanced materials, 14, no. 3 (2002): 215-218.
28. Kim, Sang-Woo, Shizuo Fujita, and Shigeo Fujita. "ZnO nanowires with high aspect ratios grown by metalorganic chemical vapor deposition using gold nanoparticles." Applied Physics Letters, 86, no. 15 (2005): 153119.
29. Vayssieres, Lionel, Karin Keis, Sten-Eric Lindquist, and Anders Hagfeldt. "Purpose-built anisotropic metal oxide material: 3D highly oriented microrod array of ZnO." The Journal of Physical Chemistry B, 105, no. 17 (2001): 3350-3352.
30. Hu, J. Q., X. L. Ma, Z. Y. Xie, N. B. Wong, C. S. Lee, and S. T. Lee. "Characterization of zinc oxide crystal whiskers grown by thermal evaporation." Chemical physics letters, 344, no. 1-2 (2001): 97-100.
31. Ghafouri, Vahid, Akbar Ebrahimzad, and Mohsen Shariati. "The effect of annealing time and temperature on morphology and optical properties of ZnO nanostructures grown by a self-assembly method." Scientia Iranica, 20, no. 3 (2013): 1039-1048.
32. Lahewil, Abdulwahab Salem Zaroug, Naser M. Ahmed, and Nurul Zahirah Noor Azman. "Structural and optical properties of ZnO nanoflakes/Al/glass

via laser-assisted chemical bath deposition (LACBD) technique." Applied Physics A, 127, no. 11 (2021): 1-8.

33. Lahewil, Abdulwahab SZ, Y. Al-Douri, U. Hashim, and N. M. Ahmed. "Structural and optical investigations of cadmium sulfide nanostructures for optoelectronic applications." Solar Energy, 86, no. 11 (2012): 3234-3240.
34. Lahewil, Abdulwahab SZ, Y. Al-Douri, U. Hashim, and N. M. Ahmed. "Structural, analysis and optical studies of cadmium sulfide nanostructured." Procedia engineering, 53 (2013): 217-224.
35. Lahewil, Abdulwahab SZ, Y. Al-Douri, U. Hashim, and Naser Mahmoud Ahmed. "Structural and morphological studies of cadmium sulfide nanostructures." In Advanced Materials Research, vol. 795, pp. 228-232. Trans Tech Publications Ltd, 2013.
36. Huang, Jinyu, Jiaxi Zhou, Zhenhua Liu, Xuejin Li, YoufuGeng, Xiaoqing Tian, Yu Du, and Zhengfang Qian. "Enhanced acetone-sensing properties to ppb detection level using Au/Pd-doped ZnO nanorod." Sensors and Actuators B: Chemical, 310 (2020): 127129.
37. Zhang, C. M., T. Meng, S. Y. Yao, S. Huang, and D. D. Wang. "Effect of Synthesis Conditions on the Growth of ZnO Nanorods via the Solution Deposition Method." International Conference on Power Electronics and Energy Engineering PEEE, (2015): 219-221.
38. Young, Sheng-Joue, and Yen-Lin Chu. "Characteristics of Field Emitters on the Basis of Pd-Adsorbed ZnO Nanostructures by Photochemical Method." ACS Applied Nano Materials, 4, no. 3 (2021): 2515-2521.
39. Ye, Zhefei, Jinze Li, Mingjun Zhou, Huiqin Wang, Yue Ma, PengweiHuo, Longbao Yu, and Yongsheng Yan. "Well-dispersed nebula-like ZnO/CeO2@ HNTs heterostructure for efficient photocatalytic degradation of tetracycline." Chemical Engineering Journal, 304 (2016): 917-933.

40. Khalafi, Tariq, FoadBuazar, and Kamal Ghanemi. "Phycosynthesis and enhanced photocatalytic activity of zinc oxide nanoparticles toward organosulfur pollutants." Scientific reports, 9, no. 1 (2019): 1-10.
41. Xiangcun Li, Gaohong He, Gongkui Xiao, Hongjing Liu, Mei Wang, Synthesis, and morphology control of ZnO nanostructures in microemulsions, Journal of Colloid and Interface Science, 333, (2009), 465-473.
42. Das, Abinash, and Ranjith G. Nair. "Effect of aspect ratio on photocatalytic performance of hexagonal ZnO nanrods." Journal of Alloys and Compounds, 817 (2020): 153277.
43. Das, Abinash, P. Malakar, and Ranjith G. Nair. "Engineering of ZnO nanostructures for efficient solar photocatalysis." Materials Letters, 219 (2018): 76-80.
44. Umar, Ahmad, Caue Ribeiro, A. Al-Hajry, Yoshitake Masuda, and Y. B. Hahn. "Growth of highly c-axis-oriented ZnO nanorods on ZnO/glass substrate: growth mechanism, structural, and optical properties." The Journal of Physical Chemistry C, 113, no. 33 (2009): 14715-14720.
45. Lai, Youlei, Ming Meng, Yifu Yu, Xitao Wang, and Tong Ding. "Photoluminescence and photocatalysis of the flower-like nano-ZnO photocatalysts prepared by a facile hydrothermal method with or without ultrasonic assistance." Applied Catalysis B: Environmental, 105, no. 3-4 (2011): 335-345.
46. Look, David C. "Recent advances in ZnO materials and devices." Materials Science and Engineering: B, 80, no. 1-3 (2001): 383-387.
47. Zyoud, S. H., Ahmed, N. M., Lahewil, A. S. Z., & Omar, A. F. B. (2022). Micro spot ZnO Nanotubes Using Laser Assisted Chemical Bath Deposition: A Low-Cost Approach to UV Photodetector fabrication. Sensors and Actuators A: Physical, 113485.

48. Moumen, Abderrahim, Navpreet Kaur, Nicola Poli, Dario Zappa, and Elisabetta Comini. "One dimensional ZnO nanostructures: Growth and chemical sensing performances." Nanomaterials, 10, no. 10 (2020): 1940.
49. Vincenzina, Strano, MariaGrazia Greco, Enrico Ciliberto, and Salvo Mirabella. "ZnO Microflowers Grown by Chemical Bath Deposition: A Low-Cost Approach for Massive Production of Functional Nanostructures." Chemosensors, 7, no. 4 (2019): 62.
50. Boruah, Buddha Deka. "Zinc oxide ultraviolet photodetectors: rapid progress from conventional to self-powered photodetectors." Nanoscale Advances, 1, no. 6 (2019): 2059-2085.
51. Al-Hilli, Safaa, and Magnus Willander. "The pH response and sensing mechanism of n-type ZnO/electrolyte interfaces." Sensors, 9, no. 9 (2009): 7445-7480.
52. Das, Abinash, S. K. Nikhil, and Ranjith G. Nair. "Influence of surface morphology on photocatalytic performance of zinc oxide: a review." Nano-Structures& Nano-Objects, 19 (2019): 100353.
53. Li, Yuqiang, Zheng, W., & Huang, F. (2020). All-silicon photovoltaic detectors with deep ultraviolet selectivity. PhotoniX, 1(1), 1-11.